Journal of Molecular Catalysis A: Chemical 314 (2009) 28–34

Contents lists available at ScienceDirect

Journal of Molecular Catalysis A: Chemical

journal homepage: www.elsevier.com/locate/molcata

A theoretical study of cyclopentene (c-C_5H_8) dehydrogenation to cyclopentadienyl anion (c-$C_5H_5^-$) on Ni (1 1 1)

Estefanía Germán, Ignacio López-Corral, Alfredo Juan, Graciela Brizuela*

Departamento de Física, Universidad Nacional del Sur, Av. Alem 1253, 8000 Bahía Blanca, Argentina

ARTICLE INFO

Article history:
Received 15 December 2008
Received in revised form 15 August 2009
Accepted 17 August 2009
Available online 22 August 2009

Keywords:
Ni (1 1 1)
Cyclopentene
Dehydrogenation
Bonding

ABSTRACT

The cyclopentene (c-C_5H_8) dehydrogenation to cyclopentadienyl anion (c-$C_5H_5^-$) on Ni (1 1 1) is studied using density functional theory (DFT) calculations. The Ni (1 1 1) surface was modeled through a unit cell of 64-atoms, while the preferred site and adsorption geometry corresponding to reactants and products were taken from previous works. We analyzed two possible mechanisms of reaction: a simultaneous dehydrogenation reaction, removing three hydrogen atoms at the same time, and a sequential dehydrogenation reaction, removing one hydrogen at a time. The geometry for each intermediate was also optimized. Results show that the sequential mechanism is kinetically favored over the simultaneous one. A bonding mechanism dominated by electron donation from H 1s orbital of cyclic intermediaries and c-$C_5H_5^-$ into the metal orbitals is also found.

1. Introduction

The adsorption of cyclic hydrocarbons and their reaction on transition metal surfaces is an intensively studied field [1–6]. The importance of these systems results from the catalytic dehydrogenation of hydrocarbons over, e.g., platinum and nickel. These dehydrogenation reactions are frequently studied in laboratories and used in high performance industrial applications, such as the nickel-based petroleum reforming process [7].

Hydrocarbon conversion chemistry over metal surfaces represents an area of significant scientific and technological interest because of its importance in catalytic reforming. At present it is widely accepted that long chain (>C_5) skeletal isomerization and dehydrocyclization reactions have the same intermediate of C_5 cyclic nature [8,9]. This topic has special interest in heterogeneous catalysts for naphtha reforming [10]. A number of experimental and theoretical studies have been considered to elucidate the structure and chemistry of such molecules on Ni and other transition metal surfaces [11–21].

Most of the experimental studies of dehydrogenation of cyclic hydrocarbons on transition metal are devoted to C_6 ring compounds, using a variety of surface analysis techniques [5,22–27]. Tjandra and Zaera obtained results from temperature-programmed desorption experiments aimed at the characterization of the thermal chemistry of C_6 cyclic hydrocarbons (cyclohexane, cyclohexene, benzene, cyclohexadienes, 1-methyl-1-cyclohexene, and toluene) and halo-hydrocarbons (iodocyclohexane, iodobenzene, and 3-bromo-cyclohexene) on Ni (1 0 0) surfaces. They found that the dehydrogenation of cyclohexene always gives benzene in high yields. This reaction proceeds via the formation of cyclohexadiene, but quite likely involves the previous formation of a C_6H_9 allylic species. Indeed, this latter reaction is facile in organometallic compounds, because the allylic C–H bond is quite weak, about 20 kcal/mol weaker than the vinylic C–H bond [26].

Papp et al. studied the interaction of cyclohexene with a Ni (1 1 1) surface using in situ high-resolution X-ray photoelectron spectroscopy at different temperatures and the thermal evolution of the corresponding layers by temperature-programmed X-ray photoelectron spectroscopy as well as temperature-programmed desorption [28].

On the other hand, the structures and reactivities of various cyclic C_5 and C_6 hydrocarbons (cyclopentene, cyclopentadiene, cyclohexene, 1,3-cyclohexadiene, and 1,4-cyclohexadiene) adsorbed on Pt (1 1 1) have been examined by means of reflection–absorption infrared (RAIR) spectroscopy [29]. Delbecq et al. studied the adsorption of cyclohexene (C_6H_{10}) on Pt (1 1 1) and two ordered Pt*n*Sn/Pt (1 1 1) surface alloys experimentally using high-resolution electron energy loss spectroscopy (HREELS), low-energy electron diffraction (LEED), and temperature-programmed desorption (TPD) as well as theoretically by ab initio density functional theory (DFT) calculations. The authors interpreted the variations in the HREELS spectra when the flash temperature increased by the formation of some dehydrogenated products. They found hydrogen desorption peaks at temperatures which can easily be assigned to the stepwise dehydrogenation of cyclohexene to benzene [30].

* Corresponding author. Tel.: +54 291 4595142; fax: +54 291 4595142.
E-mail address: brizuela@criba.edu.ar (G. Brizuela).

1381-1169/$ – see front matter © 2009 Elsevier B.V. All rights reserved.
doi:10.1016/j.molcata.2009.08.013

Several years ago, Brizuela and Castellani studied the dehydrogenation of cyclopentene on Pt (1 1 1) using the semiempirical ASED-MO theoretical method [20]. Recently, Tsuda et al. [31] investigated the cyclohexane dehydrogenation with transition metal atoms by DFT and found that a Pt atom exhibited the highest activity in breaking the C–H bond of the cyclohexane, the σ donation dominates for Pd and Cu atoms as compared with the Pt atom, and the π back-donation dominates for a Ni atom as compared with the Pt atom. The results indicate that the excess charge transfer requires more energy for breaking the C–H bond of the cyclohexane with the Pd, Ni and Cu atoms.

Saeys et al. analyzed an ab initio reaction path for benzene hydrogenation to cyclohexane on Pt (1 1 1) [32]. In other work the same authors studied the benzene dehydrogenation on Pt (1 1 1) using density functional theory (DFT), considering the addition and removal of the first two hydrogen atoms [33]. Morin et al. [34] investigated the intermediates in the reverse reaction, hydrogenation of benzene to cyclohexene, on Pt (1 1 1) and Pd (1 1 1) with DFT calculations.

Tsuda et al. also investigated spin polarization effects on cyclohexane dehydrogenation using a Ni atom as a test catalyst, by performing DFT-based total energy calculations. They compared the results with those of the well known catalyst Pt. Cyclohexane is initially adsorbed on M (M: Ni and Pt), and then becomes dehydrogenated; i.e., the axial-H atom of the cyclohexane is extracted towards the M. Unlike the singlet cyclohexane/Ni system, no energy is required to separate cyclohexyl intermediate (C_6H_{11}) from the H–Ni system for the triplet cyclohexane/Ni system. Their results suggest that the catalytic reactivity of spin-polarized Ni becomes close to that of Pt, which is considered to be, up to now, the best catalyst for cyclohexane dehydrogenation [35]. Recently Mittendorfer and Hafner developed a DFT study on the hydrogenation of benzene to cyclohexadiene on Ni (1 1 1) [36].

The objective of the present work is to study the dehydrogenation reaction of cyclopentene (c-C_5H_8) to cyclopentadienyl anion (c-$C_5H_5^-$) on Ni (1 1 1) surface and to compare two possible reaction pathways. analyzing at the same time the chemical bonding between adsorbed intermediaries species.

2. Theoretical method and adsorption model

The adsorption geometry was determinate using the Amsterdam Density Functional 2000 package (ADF-BAND2000) [37]. Gradient-corrected density functional theory (GC-DFT) calculations were performed on a supercell containing 64 atomic sites in a cubic FCC lattice to model the Ni surface by a two-dimensional slab of finite thickness, so as to better simulate the semi-infinite nature of the metallic surface. A four-layer slab was employed as a compromise between computational economy and reasonable accuracy, for the structures, the geometry optimization included all degrees of freedom of the adsorbed molecule and of the two uppermost metal layers. The molecule was adsorbed on one side of the slab with a $4 \times 4 \times 4$ reciprocal space grid in the supercell Brillouin zone [38–40]. The molecular orbitals were represented as linear combinations of Slater functions. We used the gradient correction approximation of Becke [41] for the exchange energy functional and the B3LYP [42] approximation for the correlation functional. In order to increase the computational efficiency, the innermost atomic shells of electrons are kept frozen for every atom except hydrogen, since the internal electrons do not contribute significantly to the bonding. We used a triple-zeta basis set (this means three Slater-type functions for each atomic valence orbital occupied) with polarization functions to express the atomic orbitals of Ni. The basis set of Ni consisted of 3p-, 3d- and 4s-orbitals. The *k*-points set were generated according to the geometrical method of Ramirez and Böhm [43,44]. The adsorption energies have been calculated with the following total energy difference:

$$\Delta E_{ads} = E(C_5H_n/Ni) - E(C_5H_n) - E(Ni), \quad (n = 5\text{–}8)$$

where $E(C_5H_n/Ni)$, $E(C_5H_n)$ and $E(Ni)$ are the molecular energy on the slab, the molecular energy and the bare slab energy, respectively [18].

The density of states (DOS) of both c-C_5H_n and Ni surface and the crystal orbital overlap population (OPDOS) curves between atoms and orbitals were calculated in order to analyze the adsorbate–substrate interactions. The DOS curve is a plot of number of orbitals per unit volume per unit energy. The OPDOS curve is a plot of the overlap population weighted DOS versus energy. Integration of the OPDOS curve up to the Fermi level (E_F) gives the total overlap population of the bond specified [45,46]. Looking at the OPDOS, we may analyze the extent to which specific states contribute to a bond between atoms or orbitals. The overlap population (OP) shows the degree of bonding of two specified atoms. A positive number means a bonding interaction, while a negative number means an antibonding interaction. When computing the DOS and OPDOS the system is divided into two fragments, consisting of the surface and adsorbate, respectively. This enables us to compare the changes between the bare surface, the adsorbate, and the composite adsorbed system [47]. Integration of the OPDOS curve up to the Fermi level gives the total OP.

A geometrical optimization of a cluster model for c-C_5H_8 and c-$C_5H_5^-$ on Ni (1 1 1) was carried out previously using the ADF and ASED-MO methods [48,49]. For each species, reactant, product and intermediaries, the ring-surface distance (d_{C5-Ni}) and geometry was optimized to get the total minimum energy and hence to establish the adsorption site preference.

In the present work we considered two possible dehydrogenation mechanisms. In the first one, three hydrogen atoms (H2, H4 and H6, see Fig. 1) were abstracted sequentially. In the second one they were abstracted simultaneously. During dehydrogenation reaction we also considered that three abstracted hydrogen atoms (H2, H4 and H6) finally located on the nearest hollow sites on the metallic surface.

In the case of the sequential mechanism we considered three alternatives according to the order of hydrogen abstraction. In these alternative routes we elongated different C–H bonds of the c-C_5H_8 molecule, adsorbed at the most favored site. At the same time we optimized the geometry belonging to the c-C_5H_7 intermediary. After that, we elongated other C–H saturated bonds of the optimized c-C_5H_7 intermediate and at the same time we optimized the geometry corresponding of the c-C_5H_6 intermediary. Then, we elongated the last C–H saturated bond of the optimized c-C_5H_6 intermediary and finally we optimized the geometry corresponding to the product, c-$C_5H_5^-$.

In the case of the simultaneous mechanism of reaction, all hydrogen atoms were transferred concurrently to the next hollow sites, according to a procedure which involved at the same time three C–H bond elongating, and angles optimizations for the C_5 ring.

3. Results and discussion

3.1. Adsorption geometries

The c-C_5H_8 molecule adsorbed in the most favored site and angles of the C_5 ring can be seen in Fig. 1. The c-$C_5H_5^-$ specie presents a geometric orientation which is nearly parallel to the Ni surface as displayed in Fig. 2. The equilibrium chemisorption geometries for the reactant (c-C_5H_8) and the product (c-$C_5H_5^-$) and also for intermediates during dehydrogenation at the Ni surface are

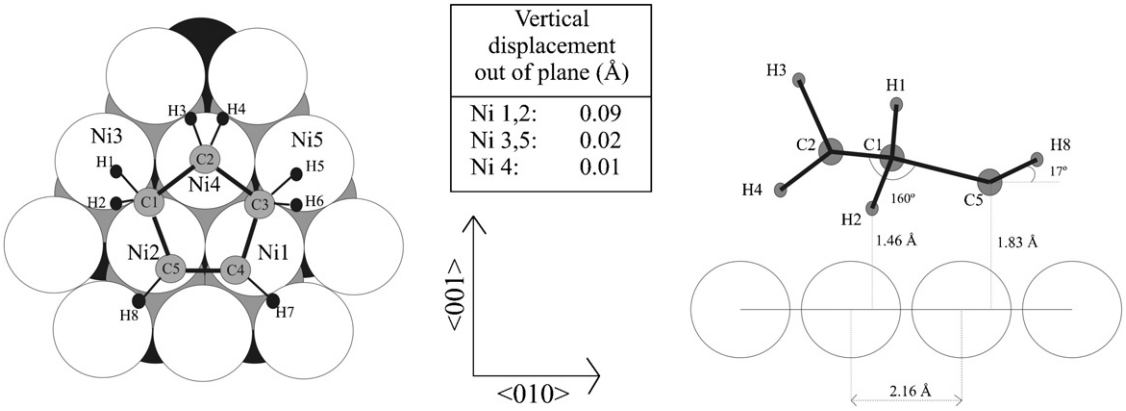

Fig. 1. (a) Preferred adsorption site of cyclopentene on Ni (1 1 1) surface (three-coordinated hollow). (b) Side view of C_5H_8 geometry after adsorption.

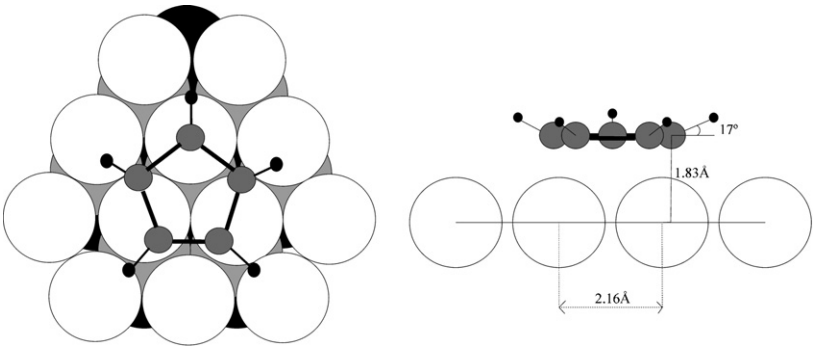

Fig. 2. (a) Preferred adsorption site of cyclopentadienyl anion on Ni (1 1 1) surface (three-coordinated hollow). (b) Side view of $C_5H_5^-$ geometry after adsorption.

listed in Table 1. Our results agree with those reported by Mittendorfer and Hafner [36]. They found carbon atom-surface distances for C_6-rings on Ni (1 1 1) between 1.81 Å and 2.74 Å depending on the intermediate and species adsorption geometry.

In Fig. 3 we can see a top and side view corresponding to the optimum geometry for the adsorbed intermediaries on Ni (1 1 1) for the different alternatives routes during dehydrogenation.

The product of the dehydrogenation reaction, c-$C_5H_5^-$, binds to the surface with its five C atoms above mainly three Ni atoms. The interaction between c-$C_5H_5^-$ and Ni (1 1 1) is very strong. The ring lays parallel to the surface, while the C–H bonds bend away 17° from the metal. This H-bending makes the C_5 carbon ring closer to the Ni (1 1 1) surface. The preferred site for the adsorption is 3CT (three-coordinated tetrahedral), with a ring-surface distance equal to 1.83 Å. The Ni–Ni bond of the surface and the C–C bonds of the cyclopentadienyl anion are weakened after adsorption when compared with the free molecule in the gas phase and the bare surface. We found that Ni d_z^2 orbitals and C p_z orbitals (normal to the surface) play an important role in the bonding between c-$C_5H_5^-$ and the surface [48]. Recently, Becker et al. [50] pointed out the importance of surface relaxation during adsorption of ethane and cyclopentene on Pt and Pt–Sn surfaces. The values of the vertical (out of plane) displacement of the Ni atoms due to chemisorption are given in Fig. 1.

On the other hand, c-C_5H_8 attaches to the surface on a 3CT (three-coordinated tetrahedral) site, with a minimum C–Ni (C5 and C4, both from the C=C) distance equal to 1.83 Å. This adsorbed molecule adopts a tilted structure in which the olefinic carbon atoms are closer to the surface than the other carbon atoms, establishing an angle equal to 160° between the non-equivalent carbon atoms. A decrease in the C=C, C–H and Ni–Ni bonds strength was observed, and the formation of =C–Ni and H–Ni bonds was detected after adsorption, describing the basic interactions during chemisorption. We also found that the Ni s, p_z and d_z^2 orbitals, the

Table 1
Equilibrium adsorption geometries for intermediaries during dehydrogenation.

Species	Site	d_{C-Ni} (Å)					d_{H-Ni} (Å)							
		C1	C2	C3	C4	C5	H1	H2	H3	H4	H5	H6	H7	H8
c-C_5H_8	3CT	2.18	2.25	2.17	1.83	1.83	3.19	1.31	3.36	1.44	3.21	1.30	2.07	2.07
c-C_5H_7 (H2)[a]	3CT	2.05	2.25	2.17	1.83	1.83	2.64	–	3.36	1.44	3.21	1.30	2.07	2.07
c-C_5H_7 (H4)[b]	3CT	2.18	2.06	2.17	1.83	1.83	3.19	1.31	2.71	–	3.21	1.30	2.07	2.07
c-C_5H_6 (H2, H6)[c]	3CT	2.05	2.25	2.06	1.83	1.83	2.64	–	3.36	1.44	2.70	–	2.07	2.07
c-C_5H_6 (H2, H4)[d]	3CT	2.00	1.98	2.17	1.83	1.83	2.67	–	2.66	–	3.21	1.30	2.07	2.07
c-$C_5H_5^-$	3CT	1.93	1.91	1.96	1.83	1.83	2.63	–	2.63	–	2.66	–	2.07	2.07

[a] Geometry of c-C_5H_7 after abstracting H2.
[b] Geometry of c-C_5H_7 after abstracting H4.
[c] Geometry of c-C_5H_6 after abstracting H2 and H6.
[d] Geometry of c-C_5H_6 after abstracting H2 and H4.

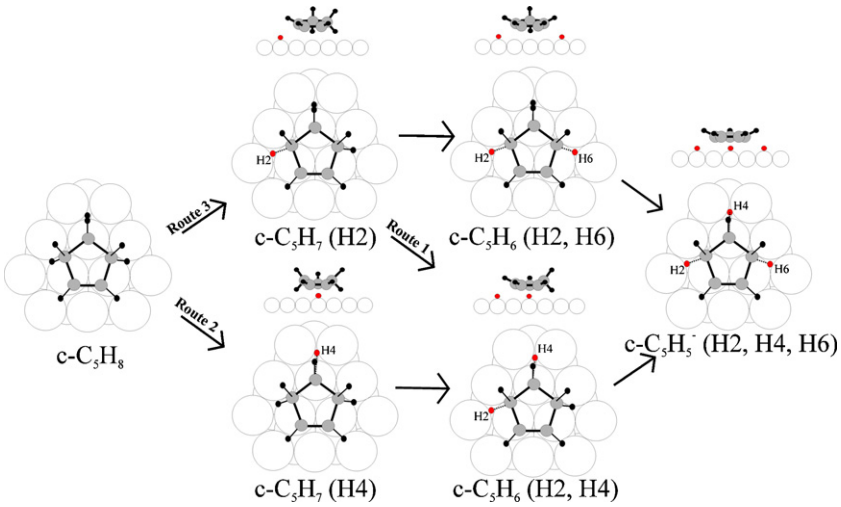

Fig. 3. Three different routes for c-$C_5H_8 \rightarrow$ c-$C_5H_5^-$ sequential dehydrogenation mechanism: route 1 (H2, H4, H6); route 2 (H4, H2, H6); and route 3 (H2, H6, H4). We have indicated which hydrogen is abstracted following the labels in Fig. 1.

C s and p_z orbitals (normal to the surface) and the H 1s orbital play an important role in the bonding between c-C_5H_8 and the surface [49].

Both cyclopentene and cyclopentadienyl anion are adsorbed on the surface at the same site (3CT) and at the same C–Ni final distance (1.83 Å). In fact, the location of the carbons of the double bond (C5=C4) remains at the same minimum C–Ni distance during all the dehydrogenation reaction, as shown in Table 1.

3.2. Dehydrogenation reaction

As mentioned before, we considered two different reaction mechanisms: simultaneous and sequential. For the simultaneous dehydrogenation reaction, we abstract three hydrogen atoms bonded to saturated carbon atoms (H2, H4 and H6 in Fig. 1) from the cyclopentene ring and locate them on the nearest tetrahedral or octahedral hollow. For the sequential dehydrogenation mechanism we explored three possible sequential routes: 1 (H2, H4, H6); 2 (H4, H2, H6); and 3 (H2, H6, H4), as shown in Fig. 3. The main difference among the three alternatives is based on the intermediary geometries during reaction. The energy vs. reaction coordinate curves obtained for each mechanism are displayed in Fig. 4 and the computed activation energies are listed in Table 2.

The dotted line in Fig. 4 shows the energy vs. reaction coordinate curve for the simultaneous dehydrogenation reaction mechanism.

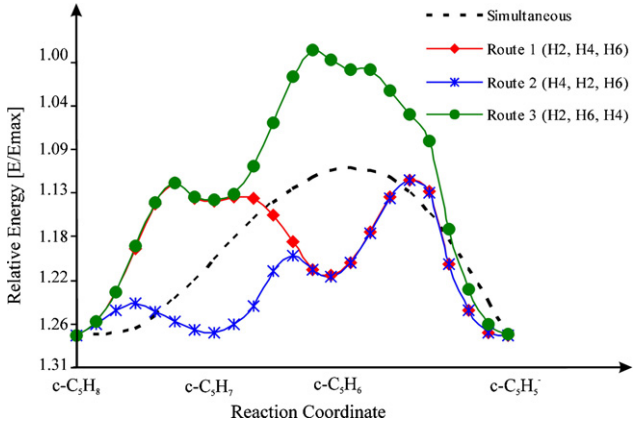

Fig. 4. Energy vs. reaction coordinate curves for simultaneous and sequential mechanisms.

The reactant and product adsorption energies are very close, cyclopentadienyl anion being more stable, so therefore the reaction becomes exothermic. Fig. 4 also shows the energy vs. reaction coordinate plot for the route 1 (H2, H4, H6) during the sequential mechanism. The abstraction of the first hydrogen (H2) presents an activation energy barrier of 0.69 eV and is finally located in a tetrahedral hole. The abstraction of the second hydrogen (H4) has a much lower energy barrier (0.02 eV) and is located in an octahedral hole. The last abstracted hydrogen (H6), which is geometrically equivalent to H2, requires an energy of 0.44 eV and is located in a tetrahedral hole. In the case of route 2 (H4, H2, H6), the mechanism starts with the abstraction of H4 having an activation energy barrier of 0.14 eV. H4 is moved to an octahedral hollow site and then H2 and H6 are moved towards tetrahedral hollow sites with activation energies barriers of 0.48 eV and 0.44 eV, respectively. Finally, for route 3 (H2, H6, H4), the hydrogen abstraction scheme is similar to those for routes 1 and 2. However, the activation energy barriers for H2 and H6 are the highest for this step (see Table 2), while H4 abstraction has almost no activation energy barrier. As can be noted from Fig. 4, the behavior of the geometrically equivalent hydrogens (H2 and H6) and the non-equivalent hydrogen (H4) is similar for the three routes of the sequential mechanism.

Regarding a kinetic analysis, we can assume that the reaction follows an Arrhenius law for each step of the sequential process and also for the simultaneous mechanism. Hence, the rate-limiting step for each sequence will be the one with the highest barrier, because steps with lower barriers are fast. By comparison of activation energies specified in Table 2, it can be seen that routes 1 and 3 corresponding to the sequential pathway have the same rate-determining step, i.e., the first hydrogen abstraction and formation of c-C_5H_7, with an energetic barrier of about 0.70 eV. The activation energy for the same step is 0.56 eV smaller in route 2, and in this sequence the rate-determining step can be identified as the second dehydrogenation step, i.e., the formation of the c-C_5H_6, with an energetic barrier of 0.48 eV.

The simultaneous mechanism has an activation energy of 0.77 eV. By looking at Fig. 4, it is obvious that the total barrier for routes 1, 2 and the simultaneous process are nearly identical. However, in the sequential mechanism, each intermediate forgets about its past once it is formed, and as a consequence the activation barrier for the rate-determining step in each sequential route becomes smaller than the barrier for the simultaneous process. In other words, from a kinetic point of view the activation energy for the

Table 2
Activation energies for simultaneous and sequential mechanisms.

Step	ΔE_{act} (Ev)			
	Sequential mechanism			Simultaneous mechanism
	Route 1 (H2, H4, H6)	Route 2 (H4, H2, H6)	Route 3 (H2, H6, H4)	
Formation of c-C_5H_7	0.69	0.14	0.70	0.77
Formation of c-C_5H_6	0.02	0.48	0.69	–
Formation of c-$C_5H_5^-$	0.44	0.44	–	–

simultaneous mechanism constitutes the highest barrier involved during c-C_5H_8 dehydrogenation reaction and thus represents the least probable alternative.

Finally, as route 2 has the rate-determining step with lowest activation barrier, we can assume that this pathway is kinetically favored over the other sequential routes and the simultaneous process. Thus, the dominant reaction path seems to follow the formation of the c-C_5H_7 (H4) surface intermediate. The low energy barrier for this step can be explained because the abstracted H4 is located in an octahedral hole, while H2 and H6 are located in tetrahedral hollows which are less favorable. The removal of a lateral hydrogen atom (H2 or H6) from adsorbed c-C_5H_n species is the slowest step during the dehydrogenation processes.

The values of activation energies listed in Table 2 are comparable with that obtained by Mittendorfer and Hafner [36]. These authors found that the rate-determining step is the first hydrogenation step, with an energetic barrier of 0.7 eV. Our activation energy values are also comparable with the results obtained for the sequential dehydrogenation of cyclohexane to benzene on Ni (1 0 0) using temperature-programmed desorption (TPD) [26], whose values are between 0.32 eV and 0.44 eV.

The present DFT study does not include temperature and coverage effects on kinetics. Such type of considerations have been taken into account by Gokhale et al. to model reaction kinetics [51] and by Mei et al. who published a DFT-based kinetic Monte Carlo simulation [52].

3.3. Analysis of selected bonds during dehydrogenation reaction

Considering the hydrogen atom which is abstracted, we identified four different intermediates in the three alternatives for the sequential dehydrogenation reaction: c-C_5H_7 (H2), c-C_5H_7 (H4), c-C_5H_6 (H2, H4), c-C_5H_6 (H2, H6). Table 3 shows the changes in the OP values for selected bonds of the intermediaries adsorbed on the surface.

The OP for the C–C bonds presents different values from =C–C: 0.686 to C=C: 0.971 in the reactant molecule, but after dehydrogenation to c-$C_5H_5^-$ all the C–C bond are almost equivalent with a mean OP value of 0.823. Similarly, the C–H bonds in c-C_5H_8 present OP values from –C–H: 0.577 to =C–H: 0.751, while the product c-$C_5H_5^-$ has similar OP values for all the C–H bonds, with a mean value of 0.774. Considering the surface, the Ni–Ni bond decreases its OP value from 0.142 to 0.127 (about 10.6%) during the dehydrogenation process. In the case of C4 and C5, the C(sp^2)–Ni OP remains almost constant while the C2(sp^3)–Ni bond increases its OP from 0.104 to 0.396. This value reveals a higher interaction of the final product c-$C_5H_5^-$ with the surface, which is considered the driving force for dehydrogenation.

In c-C_5H_8, H atoms interact with the Ni surface with an OP of 0.303 for H2 and H6, and 0.122 for the non-equivalent hydrogen H4. This is reasonable because H4 distance to the closer Ni is 1.78 Å and while the others are 1.46 Å. The strength of a multicentre bonding appears to be dependent upon the H–Ni distance: when this dis-

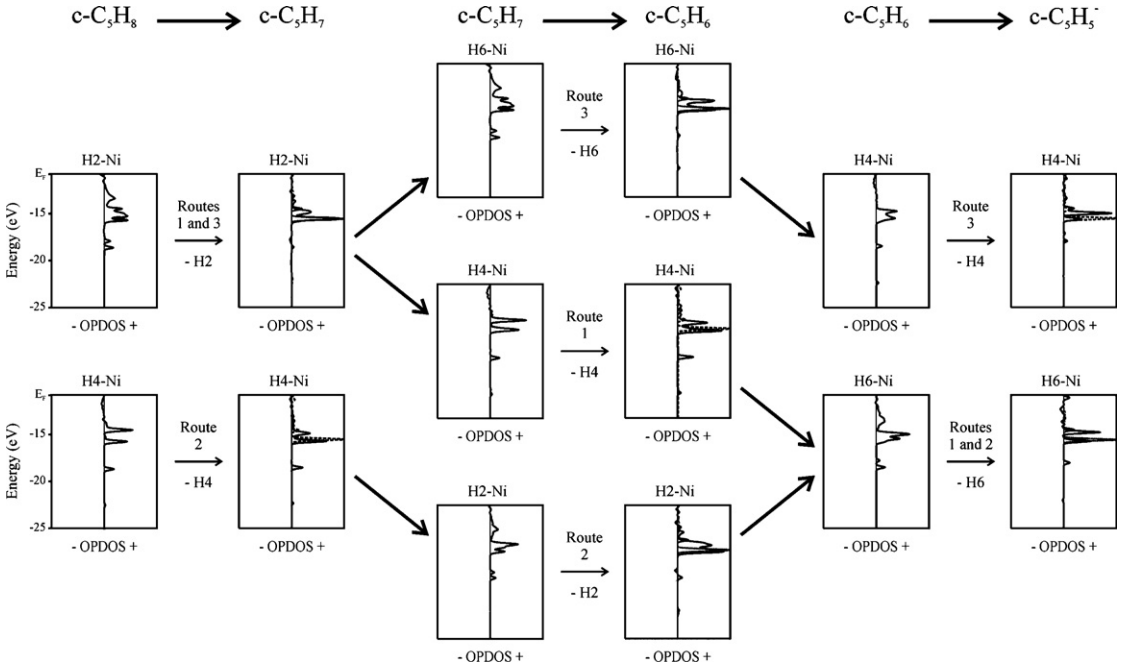

Fig. 5. OPDOS curves for H–Ni bonds between −25 eV and E_F during dehydrogenation. The dotted lines represent H–Ni on a bare Ni cluster.

Table 3
OP for selected bonds during dehydrogenation reaction (route 2).

Bonds	c-C_5H_8	c-C_5H_7	c-C_5H_6	c-$C_5H_5^-$
C1–C2	0.704	0.723	0.753	0.824
C1–C5	0.686	0.698	0.750	0.815
C4–C5	0.971	0.972	0.970	0.836
C3–C4	0.686	0.697	0.698	0.815
C2–C3	0.704	0.722	0.720	0.824
C5–H8	0.751	0.752	0.749	0.781
C4–H7	0.751	0.748	0.753	0.781
C1–H1	0.601	0.734	0.752	0.765
C1–H2	0.577	0.570	–	–
C2–H4	0.629	–	–	–
C2–H3	0.605	0.762	0.760	0.777
C3–H5	0.601	0.743	0.735	0.765
C3–H6	0.577	0.579	0.572	–
Ni1–Ni5[a]	0.142	0.139	0.138	0.127
Ni1–Ni4[b]	0.142	0.146	0.144	0.127
Ni1–Ni2[c]	0.144	0.144	0.147	0.136
C5–Ni2	0.356	0.358	0.316	0.353
C4–Ni1	0.356	0.360	0.363	0.353
C2–Ni4	0.104	0.336	0.334	0.396
H6–Ni5	0.303	0.307	0.307	0.607[d]
H4–Ni4	0.122	0.189	0.181	0.594[d]
H2–Ni2	0.303	0.307	0.181	0.607[d]

[a] Total value for the Ni–Ni OP in the free surface: 0.234.
[b] Total value for the Ni–Ni OP in the inner Ni: 0.170.
[c] Total value for the Ni–Ni OP in the bulk Ni: 0.148.
[d] Total values for the H–Ni OP at 3 fold location (H bonded to three Ni atoms, d_{Ni-H}: 1.69 Å).

Table 4
Percent change in Ni orbital population with respect to the bare cluster.

	s	p_x	p_y	p_z	d_z^2
C_5H_7 (H2)[a]					
Ni1	−26.16	−19.44	−27.73	−14.54	−19.88
Ni2	−19.23	−27.05	−39.45	−9.40	−16.86
Ni3	−14.76	−16.39	−8.76	18.61	−19.49
Ni4	−31.13	−38.40	−28.84	−34.75	−20.95
C_5H_7 (H4)[b]					
Ni1	−19.35	−24.34	−42.51	−9.50	−18.17
Ni2	−18.90	−24.13	−40.90	−10.26	−16.52
Ni3	−14.28	−17.51	−7.47	18.82	−19.66
Ni4	−28.38	−66.78	−34.94	−1.36	−26.55
C_5H_6 (H2, H4)[c]					
Ni1	−26.93	−19.93	−28.95	−18.17	−19.57
Ni2	−18.47	−26.39	−39.57	−10.07	−17.01
Ni3	−14.61	−17.99	−8.33	18.82	−19.46
Ni4	−28.89	−46.63	−35.73	−0.48	−25.74
C_5H_6 (H2, H6)[d]					
Ni1	−25.86	−20.03	−27.33	−14.54	−19.72
Ni2	−25.49	−21.33	−25.08	−13.72	−18.19
Ni3	−12.94	−8.49	−12.22	8.12	−3.09
Ni4	−30.11	−18.66	−26.64	−32.08	−20.32

[a] After H2 abstraction.
[b] After H4 abstraction.
[c] After H2 and H4 abstraction.
[d] After H2 and H6 abstraction.

tance decreases, multicentre bonding increases, and the C–H bond lengthens. The electrons in the C–H bond are attracted by the deep Ni 3d potential and delocalize into the region between the three atoms, holding them in a constrained environment. The Ni surface transfers electron density into the bonding region and is in fact slightly positively charged after adsorption. The C–H bond can be viewed as an electron donor [53].

After dehydrogenation H is finally located in three-coordinate hollow sites interacting with three Ni atoms with OP of 0.254, 0.200 and 0.153 for H2 and H6, and 0.225, 0.225 and 0.145 for H4, respectively. The overall H–Ni is increased to a value of 0.607 and 0.594, which means a strong interaction with the Ni's at 1.69 Å. The final H–Ni surface distance is 0.90 Å, which is similar to that reported in Ref. [36].

We also studied the changes in the bonding during reaction by means of OPDOS curves, shown in Figs. 5 and 6. Those curves display the evolution of H–Ni OPDOS during dehydrogenation according to the intermediaries described in Fig. 3. In all plots the H-based main peaks are above −14.6 eV, revealing some interaction with the closer C_5 intermediary if we compare this value with the OPDOS for a single H on a clean Ni surface where this peak appears at −15.5 eV. After abstractions, the bonding interaction at above −14 eV–E_F is lost. The OPDOS curves for C1–C5 and C2–Ni4 bonds are shown in Fig. 6. As mentioned before in Table 3, the OP increases from c-C_5H_8 to c-$C_5H_5^-$. C2–Ni4 bond OP also increases, as can be seen in the increased OPDOS areas between −15 eV and the E_F, and in the decreased antibonding peak at 23 eV.

Finally, Table 4 presents the percent contribution of the Ni atoms to the chemical bond with the different intermediaries. The main contribution is made by Ni 4s, 3p and $3d_z^2$ orbitals. The negative

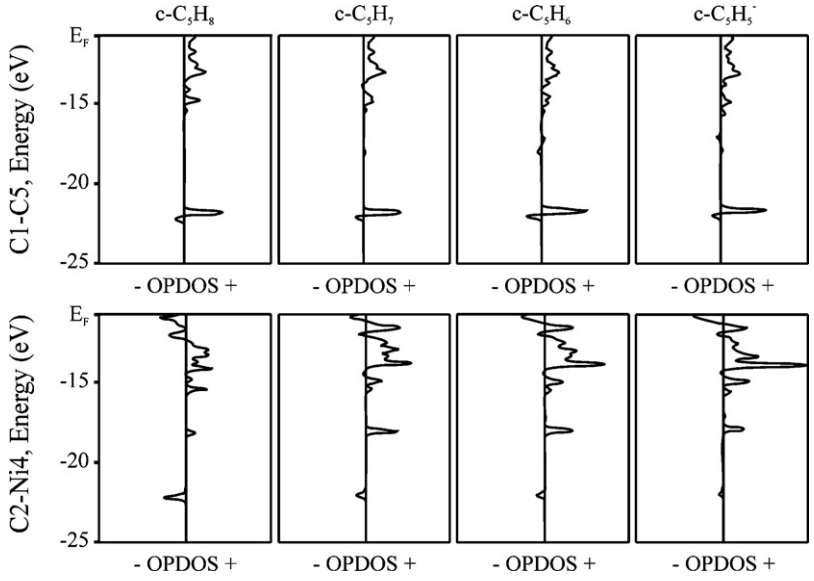

Fig. 6. OPDOS curves for C1–C5 and C2–Ni4 bonds corresponding to sequential reaction mechanism route 2.

values mean a decrease in Ni–Ni bond as already mentioned in Table 3. In a related study, Öström et al. studied the case of octane adsorbed on Cu (1 1 0) and Ni (1 1 0) and found that the position of the metal d band is important for the bonding. In effect, the interaction with the 3d band contributes to the bonding, which brings the molecule closer to the surface, thus increases the rehybridization of the molecular orbitals and allows for C–H bond activation. This is what makes Ni a better dehydrogenation catalyst. The Ni d band crosses the Fermi level, giving rise to a strong adsorbate–substrate bond [54].

4. Conclusions

In this work we studied the c-C_5H_8 to c-$C_5H_5^-$ dehydrogenation reaction on Ni (1 1 1). The results indicate that the three sequential reaction mechanisms studied are kinetically favored over a simultaneous process. In the sequential mechanism, the intermediate forgets about its past once it is formed, and as a consequence the barrier for the following step is smaller than the barrier for the simultaneous process. The reaction probability for each step will obey an Arrhenius law and the rate-limiting step will be the one with the highest barrier. Hence from a kinetic point of view the route 2 (H4, H2, H6) is the most probable sequential route. The three hydrogen atoms abstracted from saturated carbon atoms are located in hollow sites on the surface. The reaction is exothermic and the driving force to dehydrogenation seems to be the strong H–Ni bond, and the increase in the C–C and C–H bond strength in the reaction product (c-$C_5H_5^-$). From the OPDOS curves, the abstracted Hs' still present some interaction with the intermediaries when compared to a single H on a clean surface.

Acknowledgments

We thank the useful comments of the referees and the editor. Our work was supported by SGCyT-UNS-Física and PICT 1186/2006 and 560/2007. E. Germán and I. López-Corral are fellows of CONICET. A. Juan and G. Brizuela are members of that Institution.

References

[1] D. Syomin, B.E. Koel, Surf. Sci. 48 (2002) 61.
[2] D.E. Hunka, T. Picciotto, D.M. Jaramillo, D.P. Land, Surf. Sci. 421 (1999) L166.
[3] H.H. Hwu, J. Eng Jr., J. Chen, J. Am. Chem. Soc. 124 (2002) 702.
[4] C. Papp, T. Fuhrmann, B. Tränkenschuh, R. Denecke, H.P. Steinrück, Phys. Rev. B 73 (2006) 235426.
[5] D.H. Parker, C.L. Pettiette-Hall, Y. Li, R.T. McIver, J.C. Hemminger, J. Phys. Chem. 96 (1992) 1888.
[6] N.A. Khan, M.B. Zellner, L.E. Murillo, J.G.G. Chen, Catal. Lett. 95 (2004) 1.
[7] G.A. Somorjai, Introduction to Surface Chemistry and Catalysis, Wiley, New York, 1994.
[8] J.R. Anderson, Adv. Catal. 23 (146) (1973) 1.
[9] F.C. Gault, Adv. Catal. 30 (1981) 1.
[10] V. Haensel, M.J. Sterba, Adv. Chem. Ser. 5 (1951) 60.
[11] V.I. Filippov, W. Moritz, A.A. Terentjev, A.A. Vasiliev, S.S. Yakimov, IEEE Sens. J. 7 (2007) 192.
[12] W.J. Lee, C.Z. Li, Appl. Catal. A: Gen. 316 (2007) 90.
[13] Y.H. Chin, D.L. King, H.S. Roh, Y. Wang, S.M. Heald, J. Catal. 244 (2006) 153.
[14] F. Zaera, Top. Catal. 34 (2005) 129.
[15] N.C. Comelli, M.B. López, E.A. Castro, J. Mol. Struct. Theochem. 726 (2005) 197.
[16] C. Becker, F. Delbecq, J. Breitbach, G. Hamm, D. Franke, F. Jäger, K. Wandelt, J. Phys. Chem. B 108 (2004) 18960.
[17] S. Simonetti, P. Jasen, E. Gonzalez, A. Juan, G. Brizuela, Appl. Surf. Sci. 252 (2006) 7515.
[18] G. Brizuela, N.J. Castellani, Surf. Sci. 401 (1998) 297.
[19] G. Brizuela, R. Hoffmann, J. Phys. Chem. A 102 (1998) 9618.
[20] G. Brizuela, N.J. Castellani, Surf. Sci. 411 (1998) 154.
[21] G. Brizuela, N.J. Castellani, J. Mol. Catal. A: Chem. 139 (1999) 209.
[22] J.E. Demuth, H. Ibach, S. Lehwald, Phys. Rev. Lett. 40 (1978) 1044.
[23] S. Lehwald, H. Ibach, Surf. Sci. 89 (1979) 425.
[24] D.P. Land, W. Erley, H. Ibach, Surf. Sci. 289 (1993) 237.
[25] C.L.A. Lamont, M. Borbach, R. Martin, P. Gardner, T.S. Jones, H. Conrad, A.M. Bradshaw, Surf. Sci. 374 (1997) 215.
[26] S. Tjandra, F. Zaera, J. Catal. 164 (1996) 82.
[27] X.S. Ron, Y. Shen, G.A. Somorjai, Abstract of Paper of A.C.S., 213, 1997.
[28] C. Papp, R. Denecke, H.P. Streinrück, Langmuir 23 (2007) 5541.
[29] W.L. Manner, G.S. Girolami, R.G. Nuzzo, J. Phys. Chem. B 102 (1998) 10295.
[30] F. Delbecq, F. Vigné-Maeder, C. Becker, J. Breitbach, K. Wandelt, J. Phys. Chem. C 112 (2008) 555.
[31] M. Tsuda, W.A. Diño, H. Nakanishi, H. Kasai, J. Phys. Soc. Jpn. 73 (2004) 1281.
[32] M. Saeys, M.-F. Reyniers, M. Neurock, G.B. Marin, J. Phys. Chem. B 109 (2005) 2064.
[33] M. Saeys, M.-F. Reyniers, M. Neurock, G.B. Marin, J. Phys. Chem. B 107 (2003) 3844.
[34] C. Morin, D. Simon, P. Sautet, Surf. Sci. 600 (2006) 1339.
[35] M. Tsuda, W.A. Diño, S. Watanabe, H. Nakanishi, H. Kasai, J. Phys. Condens. Matter. 16 (2004) S5721.
[36] F. Mittendorfer, J. Hafner, J. Phys. Chem. B 106 (2002) 13299.
[37] Amsterdam Density Functional Package Release 2001, Vrije Universiteit, Amsterdam, 2001.
[38] P. Hohenberg, W. Kohn, Phys. Rev. 136 (1964) 864.
[39] W. Koh, L.J. Sham, Phys. Rev. 140 (1965) 1133.
[40] R.G. Parr, W. Yang, Density Functional Theory of Atoms and Molecules, Oxford University Press, New York, 1989.
[41] D. Becke, Phys. Rev. A 38 (1988) 3098.
[42] C. Lee, W. Yang, R.G. Parr, Phys. Rev. B 37 (1988) 785.
[43] R. Ramirez, M.C. Böhm, Int. J. Quantum Chem. 30 (1986) 391.
[44] R. Ramirez, M.C. Böhm, Int. J. Quantum Chem. 34 (1988) 571.
[45] G. Landrum, W. Glassey, Yet Another extended Hückel Molecular Orbital Package (YAeHMOP), Cornell University, 2004, available at http://sourceforge.net/projects/yaehmop/.
[46] R. Hoffmann, Solids and Surfaces: A Chemist's View of Bonding in Extended Structures, VCH, New York, 1988.
[47] A.W. Edith Chan, R. Hoffmann, J. Chem. Phys. 92 (1990) 1.
[48] E. Germán, S. Simonetti, M. Pronsato, A. Juan, G. Brizuela, Appl. Surf. Sci. 254 (2008) 5831.
[49] E. Germán, I. López-Corral, A. Juan, G. Brizuela, J. Mol. Catal. A: Chem. 290 (2008) 23.
[50] C. Becker, J. Haubrich, K. Wandelt, F. Delbecq, D. Loffreda, P. Sautet, J. Phys. Chem. C 112 (2008) 14693.
[51] A. Gokhale, S. Kandoi, J. Greeley, M. Mavrikakis, J. Dumesic, Chem. Eng. Sci. 59 (2004) 4679.
[52] D. Mei, P. Sheth, M. Neurock, C. Smith, J. Catal. 242 (2006) 1.
[53] A. Michaelides, P. Hu, Surf. Sci. 437 (1999) 362.
[54] H. Öström, L. Triguero, M. Nyberg, H. Ogasawara, L.G.M. Pettersson, A. Nilsson, Phys. Rev. Lett. 91 (2003) 046102–46111.